Preprint
UCRL-JC-152262

Thermodynamic Model of Afterburning in Explosions

A. L. Kuhl, M. Howard, L. Fried

This article was submitted to
34th International ICT Conference: Energetic Materials: Reactions of Propellants, Explosives and Pyrotechnics, Karlsruhe, Germany, June 24-27, 2003

April 23, 2003

U.S. Department of Energy

Lawrence
Livermore
National
Laboratory

This work was performed under the auspices of the United States Department of Energy by the University of California, Lawrence Livermore National Laboratory under contract No. W-7405-Eng-48.

34th Int. Conference of ICT
Energetic Materials, Propellants, Exposives & Pryotechnics

June 24-27, 2003
Karlsruhe, FRG

Thermodynamic Model of Afterburning in Explosions

A. L. Kuhl, M. Howard & L. Fried
University of California Lawrence Livermore National Laboratory
Livermore, California 94550

Abstract

Thermodynamic states encountered during afterburning of explosion products gases in air were analyzed with the Cheetah code. Results are displayed in the form of Le Chatelier diagrams: the locus of states of specific internal energy versus temperature, for six different condensed explosives charges. Accuracy of the results was confirmed by comparing the fuel and products curves with the heats of detonation and combustion, and species composition as measured in bomb calorimeter experiments. Results were fit with analytic functions $u = f(T)$ suitable for specifying the thermodynamic properties required for gas-dynamic models of afterburning in explosions.

1. Formulation

A theoretical model of the thermodynamic states encountered during afterburning of explosion products gases in air has been developed. The model recognizes four fluids: (*i*) oxidizer-***A*** (air), (*ii*) fuel-***F*** (expanded products gases from the detonation of fuel-rich condensed charges), (*iii*) reactants-***R***, and (*iv*), combustion products-***P***. The thermodynamic states of the fluids were evaluated by use of the Cheetah code developed by Fried (1995). While Cheetah can accommodate a variety of assumptions/models of the fluids (thermodynamic equilibrium, frozen composition, ideal gas, etc.), the correct (appropriate) thermodynamic description of each fluid was selected by comparing with bomb calorimeter experiments of Ornellas (1982).

As a proto-typical example, we consider afterburning of TNT in air (Kuhl et al, 2003). Figure 1 presents the locus of states of specific internal energy versus temperature for each of the fluids. Following Oppenheim and Kuhl (1999), we call this the *Le Chatelier* diagram* for the combustion process. The *blue* curves represent the locus of *thermodynamic-equilibrium* states of air at 1 bar (solid curves) and 10 bars (dashed curves). Below 2500 K, there is no pressure (or volume) dependence, so one can say: $u_A = u_A(T)$ in the pressure regime of interest (Kestin, 1979). The *pink* curves represent the fuel—here TNT detonation products gases expanded from

* here the absolute energy scale of the JANAF tables (Stull and Prophet, 1971) is employed.

the Chapman-Jouguet (CJ) state to one atmosphere at constant entropy (S = 1.625 Cal/g-K). The curve labeled S_e represents the equilibrium isentrope, while the curve labeled S_f corresponds to the isentrope with composition frozen as the products expand to temperatures below 1800 K.

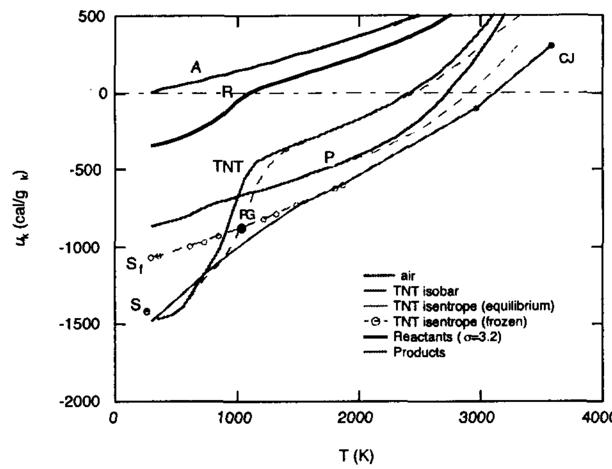

Figure 1. Locus of isobaric and isentropic states in the thermodynamic plane of specific internal energy versus temperature (solid curves = 1 bar, dashed curves = 10 bars).

The equilibrium isentrope, S_e, gives a value of –1500 Cal/g for the heat of detonation evaluated at 298 K, while the frozen curve, S_f, gives a value: -1100 Cal/g, in good agreement with the value -1093 Cal/g measured by Ornellas (1982). The *green* curves depict isobars of TNT detonation products at 1 bar (solid curve) and 10 bars (dashed curve); both approach the value of –1550 Cal/g at room temperature—in agreement with S_e, in contradiction to the measured heat of detonation of –1093 Cal/g. The compositions of the pink and green curves are presented in Table 1. The composition frozen at 1400 K shows the best agreement with data (especially for *CO*). From these comparisons we conclude that the physically appropriate curve is S_f: the locus of states corresponding to the detonation products gases expanding at constant entropy starting at the CJ point, with the composition frozen at 1400K, in agreement with Rhee *et al* (1996). The fuel curve S_f and the air curve A were combined in stoichiometric proportions ($\sigma_s = 3.2$) to form *frozen* Reactants-***R***, depicted as the black line in Fig. 1. These are transformed to combustion products-***P*** (*red* curves) assumed to be in state of thermodynamic equilibrium. Below 2500 K, there appears to be no pressure (or volume) dependence on the products curve, so again one can say: $u_P = u_P(T)$ for the combustion regime of interest (this is consistent with Chemkin [12]).

Table 1. Composition of TNT detonation products gases expanded to p = 1 bar and T = 298K along the CJ isentrope S = 1.625 Cal/g-K

Species (mol/kg)	Cheetah code (T_f = 1800K)	Cheetah code (T_f = 1400K)	Cheetah code (equilibrium)	Calorimeter (Ornellas, 1982)
CO	10.34	8.87	0.82	8.72
N2	6.53	6.57	6.6	5.81
H2O	6	5.02	5.64	7.04
CO2	5	6.25	9.5	5.50
H2	2.2	2.84	2.8	2.03
CH4	1.2	1.52	0.8	0.44
C(s)	14.16	14.16	19.67	16.1
Gas	31.58	31.16	27.13	—

Next we investigate the pressure (p)-specific volume (v)-temperature (T) behavior of the fluids. This is done by plotting the locus of states, as determined by Cheetah, of pv versus RT for afterburning of TNT as depicted in Fig. 2. We see that the results for air (*blue* curve), TNT equilibrium isobar (*green* curve) and equilibrium combustion products (*red* dots) lie along a 45 degree line—demonstrating graphically that those fluids satisfy the perfect gas (PG) equation:

$$p_k v_k = R_k T_k \tag{1}$$

The locus of states for TNT detonation products expanding down the CJ isentrope is depicted as the *pink* dashed curve. It obeys the Jones-Wilkins-Lee (JWL) relation:

$$p_{JWL} = A(1 - \varpi\rho_c / \rho R_1)e^{-R_1\rho_c/\rho} + B(1 - \varpi\rho_c / \rho R_2)e^{-R_2\rho_c/\rho} + \varpi\rho(u - u_0) \tag{2}$$

where A = 3.712 Mbars, B = 0.03231 Mbars, $R_1 = 4.15$, $R_2 = 0.95$, and $\varpi \equiv (\gamma_F - 1) = 0.39$ for TNT (Dobratz, 1974). At large RT, this locus is exponential, but at small RT (< 271 j/g) it again

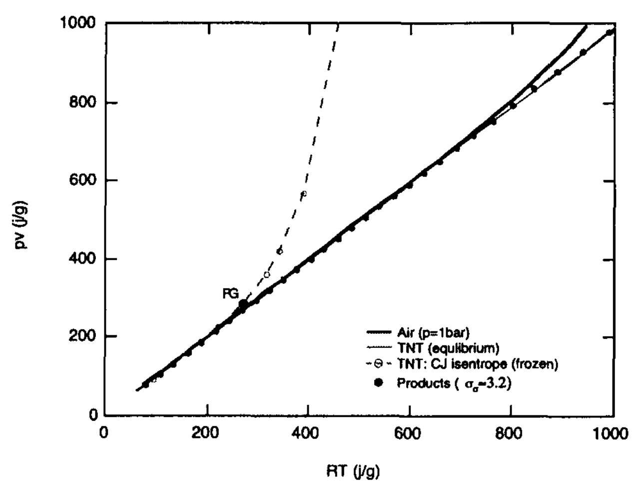

Figure 2. Locus of states in the thermodynamic plane of pv versus RT.

lies along the diagonal perfect gas line (1). This coincidence begins at the point labeled PG ($p_{PG} = 236\, bars,\ v_{PG} = 12\, cc/g, T_{PG} = 1036\, K$) in Figs. 1 and 2, and occurs when the charge radius has expanded by a factor of three or more. Thus for $p < p_{PG}$ and $T < T_{PG}$, the fuel satisfies the perfect gas equation (1).

2. Thermodynamics

Based on the above formulation, we have analyzed the thermodynamics of afterburning of detonation products gases from PETN ($C_5H_8N_4O_{12}$) and TNT ($C_7H_5N_3O_6$) charges in air. Results are presented in the form of *Le Chatelier* diagrams in Figs. 3 and 4. Points denote computed values based on the CHEETAH code, while the curves represent quadratic fits:

$$u_k(T) = a_k T^2 + b_k T + c_k \tag{3}$$

which do an excellent job of representing the computed points. Thermodynamic properties (constants a_k, b_k, c_k) corresponding to these fits, are listed in Table 20. At room temperature, the computed points are in good agreement with the measured heats of detonation and combustion (H_d and H_c) depicted in the figures. Composition of the detonation products and combustion products, as computed by CHEETAH, are also in good agreement with data (Tables 3, 4, 6 and 7), thereby spawning excellent agreement with measured H_d and H_c as shown in Tables 2 and 4. Combustion in a thermodynamically isolated chamber is represented by an iso-energy transformation $\boldsymbol{R} \rightarrow \boldsymbol{P}$ in the *Le Chatelier* plane; for reactants starting at room temperature, this is illustrated by the horizontal black line in the figures. We have also analyzed the combustion of four Shock-Dispersed-Fuel (SDF) charges (see Neuwald *et al*, 2003):

- an aluminized fuel: SDF_1 ($45\% C_4H_8N_8O_8; 35\% Al; 20\% C_4H_6$)
- a polyethylene-based fuel: SDF_2 ($17\% C_5H_8N_4O_{12}; 17\% Al; 66\% CH_2 - CH_2$)
- an IPN-based fuel: SDF_3 ($29\% C_4H_8N_8O_8; 15\% Al; 56\% C_3H_7NO_3$)
- a magnesium-based fuel: SDF_4 ($40\% Mg; 60\% C_3H_7NO_3$)

Le Chatelier diagrams for the combustion of the SDF charges in air are presented in Figs. 5-8. Their thermodynamic property constants are listed in Table 20. Theoretical heats of detonation and combustion are listed in Tables 8, 11, 14 and 17. Their heats of combustion are considerably larger than that of TNT; most notable is the value $-8{,}457\ Cal/g_{HE}$ for the polyethylene-based fuel (SDF_2). If one can induce combustion (e.g., via turbulent mixing with air), one can expect a considerable (~3) increase in afterburning effects from these fuels.

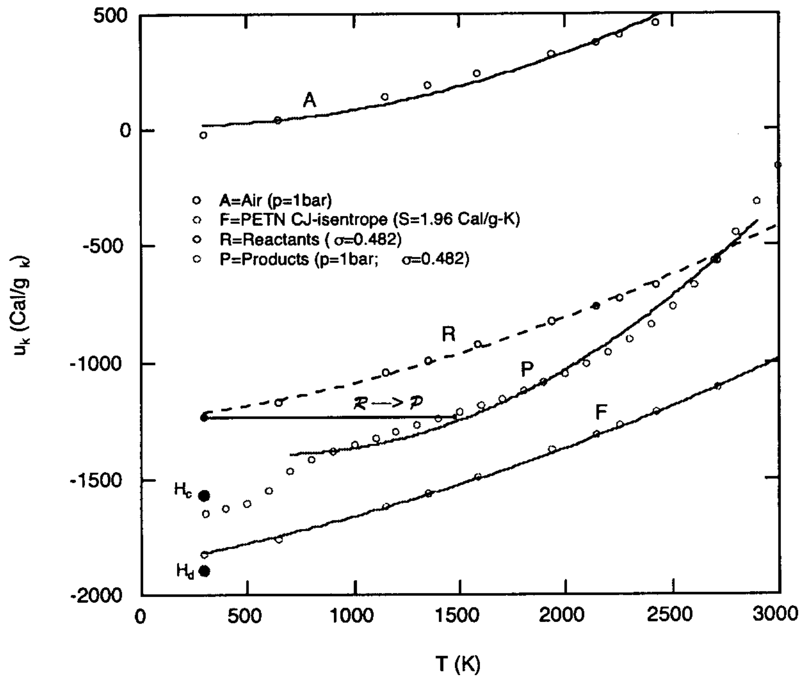

Figure 3. Le Chatelier diagram for combustion of PETN explosion products in air.

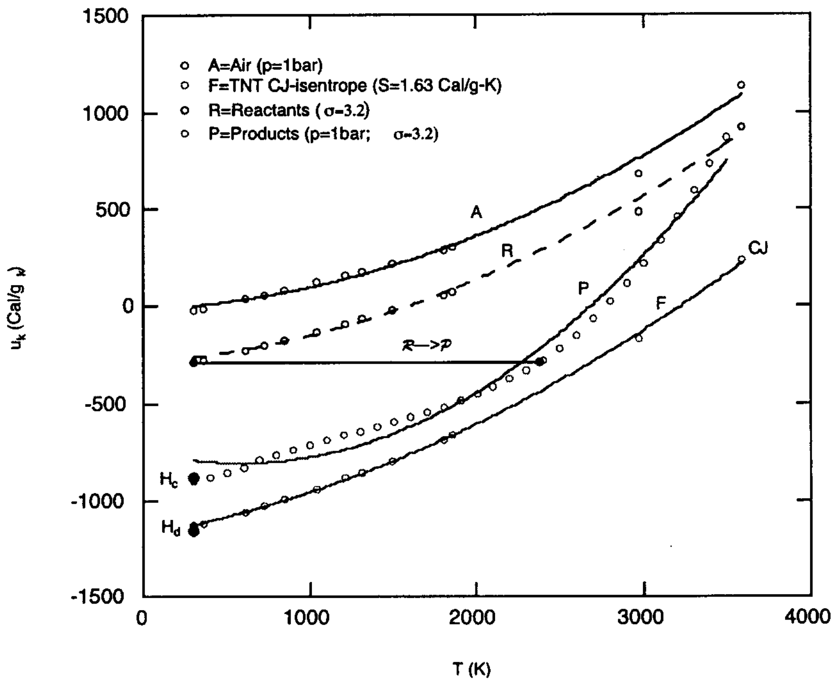

Figure 4. Le Chatelier diagram for combustion of TNT explosion products in air.

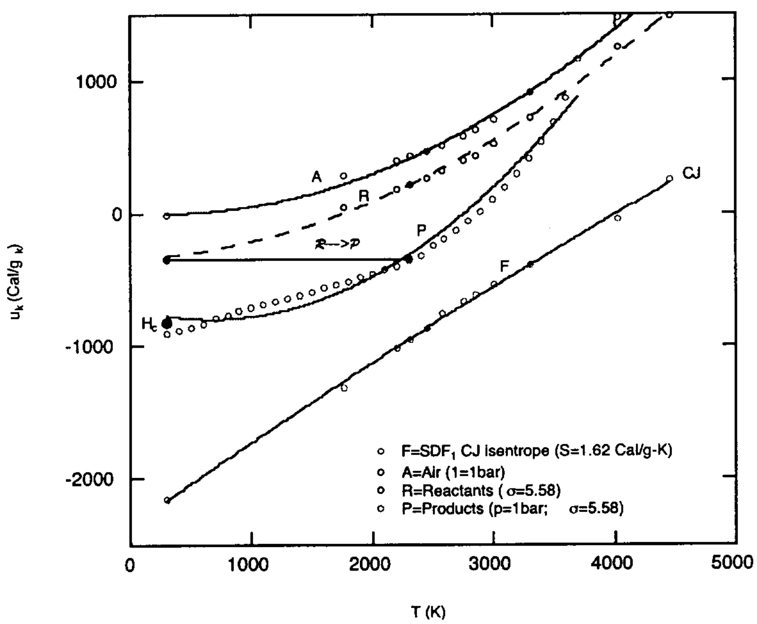

Figure 5. Le Chatelier diagram for combustion of SDF_1 explosion products in air.

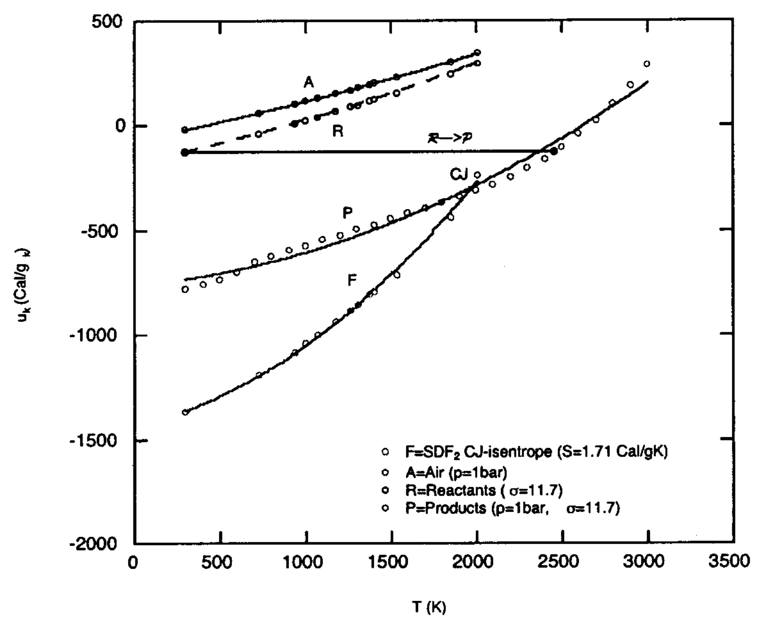

Figure 6. Le Chatelier diagram for combustion of SDF_2 explosion products in air.

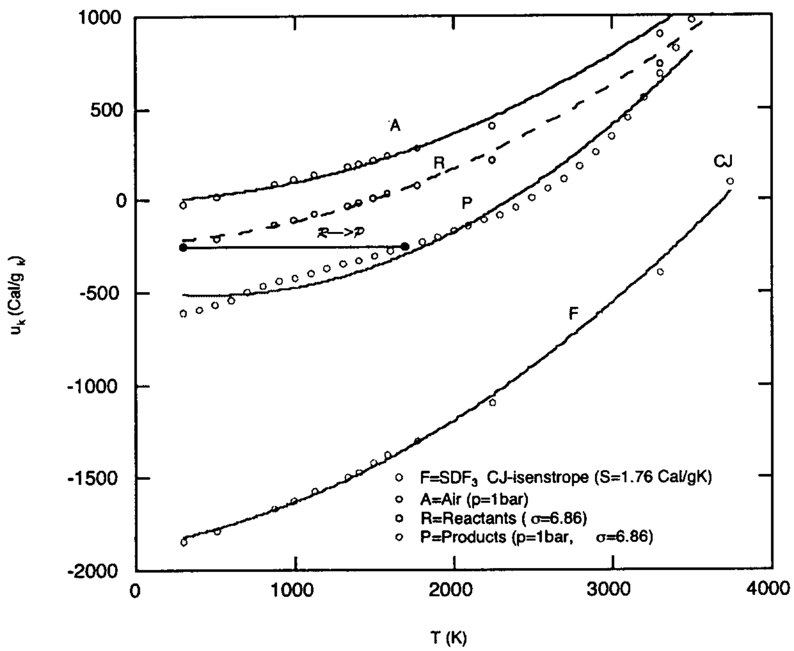

Figure 7. Le Chatelier diagram for combustion of SDF_3 explosion products in air.

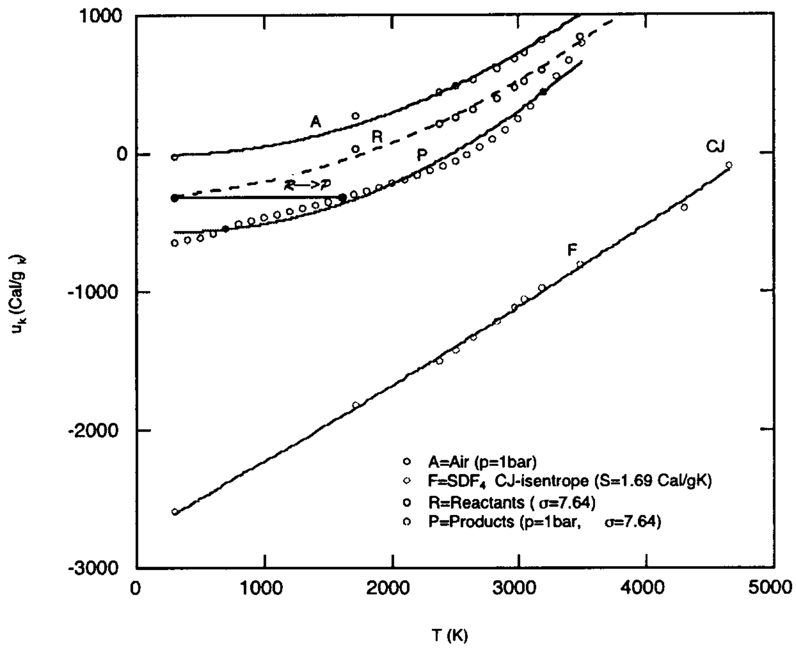

Figure 8. Le Chatelier diagram for combustion of SDF_4 explosion products in air.

3. Equations of State

Based on the Formulation of §-1, one can define equations of state for the fluids. For a pure fluid k, one can invert (3) to find the temperature as a function of specific internal energy:

$$T_k = \left[-b_k + \sqrt{b_k^2 - 4a_k(c_k - u_k)}\right]/2a_k \tag{4}$$

while the pressure is calculated from the perfect gas equation (1) or the JWL relation (2):

$$p_k = \begin{cases} \rho_k R_k T_k & (k = A,\ F\ (v > v_{PG})\ \&\ P) \\ A(1-\omega\rho_0/\rho R_1)e^{-R_1\rho_0/\rho} + B(1-\omega\rho_0/\rho R_2)e^{-R_2\rho_0/\rho} + \omega\rho(u-u_0) & (k = F\ (v < v_{PG})) \end{cases} \tag{5}$$

For a mixture (denoted by subscript m), we assume that the fluids obey the ideal thermodynamic mixing laws of mass and energy conservation:

$$\rho_m \equiv \sum_k \rho_k \tag{6}$$

$$u_m(T_m) \equiv \sum_k Y_k u_k \tag{7}$$

with their corresponding mixture properties calculated from the mass-weighted averaging:

$$a_m = \sum_k Y_k a_k \quad b_m = \sum_k Y_k b_k \quad c_m = \sum_k Y_k c_k \quad R_m = \sum_k Y_k R_k \tag{8}$$

Then the mixture temperature is calculated from mixture specific internal energy:

$$T_m = \left[-b_m + \sqrt{b_m^2 - 4a_m(c_m - u_m)}\right]/2a_m \tag{9}$$

while the mixture pressure and specific volume satisfies Dalton's law and Amagat's law:

$$p_m = \sum_k p_k = \rho_m R_m T_m \tag{10}$$

$$v_m = \sum_k v_k = R_m T_m / p_m \tag{11}$$

4. Combustion

For hydro-code modeling one can divide combustion into three fundamental steps.

Step 1—Reactants Formation: based on stoichiometric mixing of fuel and air:

mass: $$m_R = \begin{cases} m_F + \sigma_s m_F & (\sigma > \sigma_s) \\ m_A/\sigma_s + m_A & (\sigma < \sigma_s) \end{cases} \quad \& \quad m_D = m_m - m_R \tag{12}$$

energy: $$u_R(T_R) = (u_F + \sigma_s u_A)/(1+\sigma_s) \tag{13}$$

leading to the reactants temperature:

$$T_R = \left[-b_R + \sqrt{b_R^2 - 4a_R(c_R - u_R)}\right]/2a_R \tag{14}$$

where the reactants properties are known from Table 20. This is represented graphically in Fig. 21 by the *blue* lines.

Step 2—Combustion: corresponding to material transformation $\boldsymbol{R} \to \boldsymbol{P}$ in the *Le Chatelier* plane at constant mass and energy:

mass: $$m_P = m_R \tag{15}$$

energy: $$u_P = u_R \tag{16}$$

creating a products temperature determined from its specific internal energy:

$$T_P = \left[-b_P + \sqrt{b_P^2 - 4a_P(c_P - u_P)}\right]/2a_P \tag{17}$$

where the products properties are known from Table 20. This is represented graphically in Fig. 21 by the *red* lines.

Step 3—Thermal Equilibration: of the products and diluent via mixing:

mass: $$m_m = m_P + m_D \tag{18}$$

energy: $$u_m(T_m) = m_P u_P + m_D u_D \tag{19}$$

resulting in a mixture temperature determined from its specific internal energy:

$$T_m = \left[-b_m + \sqrt{b_m^2 - 4a_m(c_m - u_m)}\right]/2a_m \tag{20}$$

This is represented graphically in Fig. 9 by the *pink* lines for fuel-rich mixtures ($\sigma < \sigma_s$), and by the green lines for air-rich mixtures ($\sigma > \sigma_s$).

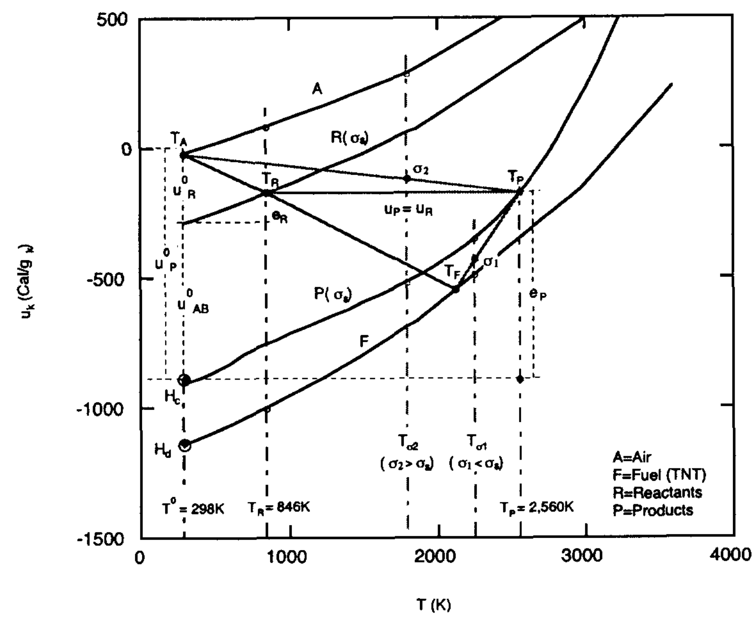

Figure 9. Combustion model showing: *i. reactants formation* (blue lines), *ii. combustion* (red lines) and *iii. thermal equilibration* (pink or green lines).

4. Conclusions

A Thermodynamic Model of the afterburning of explosion products gases in air has been developed. The locus of thermodynamic states of the fuel (detonation products) lie on an isentrope $u_F = u_F(T; S_{CJ}, n_i(T_f))$ passing through the CJ point with its composition $n_i(T_f)$ frozen at temperatures below T_f, while the locus of products states lie on the thermodynamic equilibrium curve $u_P = u_P(T; \sigma_s)$ which depends on the stoichiometry σ_s. These loci, and their associated heats of detonation and combustion and composition, are the only loci that agree with bomb calorimeter data. This means that the specific internal energy of each fluid is solely a function of temperature: $u_k = u_k(T)$ in this combustion regime, and may therefore be treated as a perfect gas (Kestin, 1979). We took advantage of this and fit the u_k curves with quadratic functions of temperature, which were used to specify the EOS and thermodynamic properties of the fluids. This methodology can be used model afterburning in a broad spectrum of SDF explosions, including metallic fuels, polyethylene-based fuels, IPN-based fuels, etc. This Model has been designed to be coupled to gas-dynamic codes to predict the evolution of afterburning in explosions (Kuhl et al, 1999) in the chemical-equilibrium limit.

Acknowledgements

This work was performed under the auspices of the U. S. Department of Energy by the University of California, Lawrence Livermore National Laboratory under Contract No. W-7405-Eng-48. It was sponsored by the Defense Threat Reduction Agency under IACRO # 01-4441 & # 02-40851.

References

[1] Fried, L. E., *CHEETAH 1.22 User's Manual*, **UCRL-MA-117541** (rev. 2), LLNL, 187 pp., 1995.
[2] Ornellas, D. L., *Calorimetric Determination of the Heat and Products of Detonation for Explosives: October 1961 to April 1982*, LLNL, **UCRL-52821**, 1982.
[3] Ree, F.H, Pitz, W.J, van Thiel, M, Souers, P.C., Over-abundance of Carbon Monoxide in Calorimeter Tests. *J. Phys. Chem.* 1996, **100**, pp. 5761-5765.
[4] Neuwald, P., Reichenbach, H., and Kuhl, A. L., Shock-Dispersed-Fuel Charges—Combustion in Chambers and Tunnels, *34th Int. Conf. Energetic Materials, Propellants, Explosives & Pyrotechnics*, ICT (in press).
[5] Kuhl, A.L, Ferguson, R.E., Oppenheim, A.K., Gasdynamics of Combustion of TNT Products in Air, *Archivum Combustionis*, **19** (1-4), 1999, pp. 67-89.
[6] Kuhl, A.L., Forbes, J.W., Chandler, J.B., Afterburning of Detonation Products from TNT Charges in a 16-m^3 Chamber, *34th Int. Conf. on Energetic Materials, Propellants, Explosives & Pyrotechnics*, ICT (in press).
[7] J. Chang, private communication, 2002.
[8] Kestin, J., *A Course in Thermodynamics, revised printing*, Vol. **I**, Hemisphere Publishing, 1979, pp. 551-559.
[9] Oppenheim, A. K., and Kuhl, A.L., Aerothermodynamics of Closed Combustion Systems, *Archivum Combustionis*, **19** (1-4), 1999, pp. 16-65
[10] Stull, D.R, and Prophet, H., *JANAF Thermochemical Tables*, National Bureau of Standards, U.S. Department of Commerce, Report NSRDS-NBS 37, 1971, 1141 pp.
[11] Dobratz, B., *Properties of Chemical Explsives and Explosive Simulants*, Lawrence Livermore National Laboratory, UCRL-**51319**, Livermore, CA, 1974.
[12] Kee, R.J., Rupley, f.M. & Miller, J.A., *1989 Chemkin-II: A Fortran Chemical Kinetics Package for the Analysis of Gas-Phase Chemical Kinetics*, **SAND89-8009B**, Sandia National Laboratories.

Table 2. Heats of detonation and combustion for a PETN charge ($C_5H_8N_4O_{12}$)

Source	ΔH_d (Cal/g_{HE})	H_d* (Cal/g_{HE})	ΔH_c (Cal/g_P)	H_c** (Cal/g_P)
Cheetah, $\rho_0 = 1g/cc$	-1,421	-1823	-1,371	-1649
Experiment (Ornellas, 1982)	-1,502	-1892	-1,292.7 (1,916 Cal/g_{PETN})	-1571

* $E_{0,PETN} = -402 Cal/g_{PETN}$ ** $E_{0,P} = -278 Cal/g_P$

Table 3. Composition of expanded PETN detonation products gases

Species	Composition (mol/mol PETN)	
	Cheetah (T_F = 2,145K)	Experiment (Ornellas, 1982)
N2	2.00	1.95—2.10
H2O	3.65	3.40—3.68
CO2	3.34	3.33—3.50
CO	1.69	1.50—1.72
H2	0.341	0.34—0.60

Table 4. Composition of combustion products of PETN in air ($\sigma = 0.4822$)

Species	Composition (mol/mol PETN)	
	Cheetah (in air)	Experiment (in O_2) (Ornellas, 1982)
N2	6.17	2.00
H2O	4.00	4.01
CO2	5.00	4.83
CO	0	0.15
H2	0	0.035

Table 5. Heats of detonation and combustion for a TNT charge ($C_7H_5N_3O_6$)

Source	ΔH_d (Cal/g_{HE})	H_d* (Cal/g_{HE})	ΔH_c (Cal/g_P)	H_c** (Cal/g_P)
Cheetah, $\rho_0 = 1.65 g/cc$	-1,069.8	-1136	-827.2 ($-3,474.4\ Cal/g_{TNT}$)	-858
Experiment, $\rho_0 = 1.53 g/cc$ (Ornellas, 1982)	-1,093 ±11	-1159	-855.7 ($-3,594 \pm 60\ Cal/g_{TNT}$)	-887

* $E_{0,TNT} = -66.3 Cal/g_{TNT}$ ** $E_{0,P} = -31.4 Cal/g_P$

Table 6. Composition of expanded TNT detonation products gases ($\rho_0 = 1.65 g/cc$)

Species	Composition (mol/kg TNT)	
	Cheetah (T_F = 1,400K)	experiment (Ornellas, 1982)
CO	8.87	8.72
N2	6.57	5.81
H2O	5.02	7.04
CO2	6.25	5.50
H2	2.84	2.03
CH4	1.52	0.44
H2Oa	-	-
C(s)	14.2	16.1
Gas	31.2	

Table 7. Composition of combustion products of TNT in air ($\sigma = 3.2$)

Species	Composition (mol/kg TNT)	
	Cheetah (in air)	Experiment (in O_2) (Ornellas, 1982)
N2	22.42	1.54
H2O	2.621	2.65
CO2	7.338	6.82
CO	0	0.38
H2	0	0.05
CH4	0	0.0011
O2	0.057	0
C(s)	0	0
Gas	32.4	

Table 8. Heats of detonation & combustion for SDF_1 ($45\% C_4H_8N_8O_8$; $35\% Al$; $20\% C_4H_6$)

Source	ΔH_d (Cal/g_{HE})	H_d* (Cal/g_{HE})	ΔH_c (Cal/g_P)	H_c** (Cal/g_P)
Cheetah ($\rho_0 = 1.70\, g/cc$)	-2,183.9	-2156	-847.7 ($-5,578\ Cal/g_{HE}$)	-861
Experiment (J. Chang, 2002)	—	—	813 ($5,347\ Cal/g_{HE}$)	-826

* $E_{0,HE} = -28.1\, Cal/g_{HE}$ ** $E_{0,P} = -13.1\, Cal/g_P$

Table 9. Composition of expanded SDF_1 detonation products gases ($\rho_0 = 1.70\, g/cc$)

Species	Composition (mol/kg SDF_1)	
	Cheetah-CJ (127kb, 4456K,)	Cheetah (1bar, 298K)
CO	0.1546	
N2	2.545	3.642
H2O	0.290	
NH3	1.833	
C2H4	1.832	
C2H6	0.4178	
H	0.278	
C2H2	0.208	
H2	3.214	
CH4	2.813	8.584
C(s)	12.91	12.28
Al2O3 (l)	3.89	4.052
AlN (s)	5.19	4.869
Total gas	13.63	12.23
Total solid	22.03	21.21

Table 10. Composition of combustion products of SDF_1 in air ($\sigma = 5.58$)

Species	Composition (mol/kg SDF_1)	
	Cheetah (1bar, 2,500K)	Cheetah (1bar, 298K)
N2	23.68	23.81
H2O	2.739	2.863
CO2	2.827	3.48
CO	0.6531	
H2	0.101	
O2	0.7836	0.5609
C(s)	0	
Al2O3 (l)	1.082	1.082
AlN (s)	0	
Total gas	31.16	30.71
Total solid	1.082	1.082

Table 11. Heats of detonation & combustion for SDF_2 ($17\% C_5H_8N_4O_{12}$; $17\% Al$; $66\% CH_2-CH_2$)

Source	ΔH_d (Cal/g_{HE})	H_d* (Cal/g_{HE})	ΔH_c (Cal/g_P)	H_c** (Cal/g_P)
Cheetah ($\rho_0 = 1.16 g/cc$)	-998.5	-1373	-668.5 ($-8,457\ Cal/g_{HE}$)	-750

* $E_{0,HE} = -374\, Cal/g_{HE}$ ** $E_{0,P} = -87.0\, Cal/g_P$

Table 12. Composition of expanded SDF_2 detonation products gases ($\rho_0 = 1.16 g/cc$)

Species	Composition (mol/kg HE)	
	Cheetah-CJ (68 kbar, 2007K)	Cheetah (1bar, 298K)
C2H4	0.1535	
N2		0.0578
H2O	0	0
CO2	0	0
H2	3.165	9.237
CH4	20.42	20.01
C2H6	1.701	0.105
C(s)	26.04	2.109
Al2O3 (s)	2.108	2.109
AlN (s)	1.962	1.96
Total gas	25.59	29.45
Total solid	30.11	34.0

Table 13. Composition of combustion products of a SDF_2 charge in air ($\sigma = 11.65$)

Species	Composition (mol/kg HE)	
	Cheetah (1bar, 2,500K)	Cheetah (1bar, 298K)
N2	25.13	25.28
H2O	3.763	3.924
CO2	3.244	3.966
CO	0.7215	
H2	0.1340	
CH4	0	
O2	0.9323	0.678
C(s)	0	
Al2O3 (l)	0.2441	0.2441
AlN (s)	0	
Total gas	34.35	33.85
Total solid	0.2441	0.2441

Table 14. Heats of detonation & combustion for SDF_3 ($29\% C_4H_8N_8O_8; 15\% Al; 56\% C_3H_7NO_3$)

Source	ΔH_d (Cal/g_{HE})	H_d* (Cal/g_{HE})	ΔH_c (Cal/g_P)	H_c** (Cal/g_P)
Cheetah ($\rho_0 = 2.01 g/cc$)	-1,571	-1846	-511 ($-4{,}020\ Cal/g_{HE}$)	-564

* $E_{0,HE} = -275 Cal/g_{HE}$ ** $E_{0,P} = -52.9 Cal/g_P$

Table 15 Composition of expanded SDF_3 detonation products gases

Species	Composition (mol/kg HE)	
	Cheetah-CJ (302 kbar, 3741K)	Cheetah (1bar, 298K)
CO		7.496
N2	3.088	6.537
H2O	13.14	4.420
CO2	0.2186	1.779
H2	0.1406	7.980
CH4	0.1663	5.002
NH3	5.204	
CHNO	1.775	
C(s)	17.49	5.602
Al2O3 (s)	2.780	2.780
Total gas	24.02	33.32
Total solid	20.27	8.382

Table 16. Composition of combustion products of a SDF_3 charge in air ($\sigma = 6.86$)

Species	Composition (mol/kg HE)	
	Cheetah (1bar, 2,500K)	Cheetah (1bar, 298K)
N2	24.45	24.72
H2O	2.800	2.870
CO2	2.262	2.531
CO	0.2686	
H2	0.05	
CH4	0	
NH3	0	
O2	3.215	3.388
C(s)	0	
Al2O3 (l)	0.3536	0.3536
Total gas	33.77	33.50
Total solid	0.3536	0.3536

Table 17. Heats of detonation & combustion for a SDF_4 ($40\%\,Mg; 60\%\,C_3H_7NO_3$)

Source	ΔH_d (Cal/g_{HE})	H_d* (Cal/g_{HE})	ΔH_c (Cal/g_P)	H_c** (Cal/g_P)
Cheetah ($\rho_0 = 1.85\ g/cc$)	-2,284	-2597	-595.5 ($-5{,}143\ Cal/g_{HE}$)	-650

* $E_{0,HE} = -313 Cal/g_{HE}$ ** $E_{0,P} = -54.5 Cal/g_P$

Table 18. Composition of expanded SDF_4 detonation products gases ($\rho_0 = 1.85\ g/cc$)

Species	Composition (mol/kg HE)	
	Cheetah-CJ (160 kbar, 4649K)	Cheetah (1 bar, 298)
H2	3.115	.0004
N2	1.1676	2.854
NH3	2.303	
CH4	3.179	9.653
C2H4	2.247	
C(s)	6.321	7.474
MgO(s)	16.45	16.45
Total gas	14.31	13.18
Total solid	24.28	23.93

Table 19 Composition of combustion products of a SDF_4 charge in air ($\sigma = 7.64$)

Species	Composition (mol/kg HE)	
	Cheetah (1 bar, 2,500K)	Cheetah (1 bar, 298K)
N2	24.3	24.5
H2O	2.26	2.31
CO2	1.78	1.98
CO	0.209	-
O2	3.15	3.35
O	0.146	3.388
MgO (s)	1.91	1.91
Total gas	32.4	32.2
Total solid	1.91	1.91

Table 20. Thermodynamic properties: $u_k(T) = a_k T^2 + b_k T + c_k$ for various charges.

charge (composition)	k	a_k (Cal/g-K^2)	b_k (Cal/g-K)	c_k (Cal/g)
Air	A	6.33 e-5	0.497	7.36
PETN ($C_5H_8N_4O_{12}$)	F	4.25 e-5	0.167	-1872
	R	5.88 e-5	0.104	-1256
	P	-19.5 e-5	-0.249	-1315
TNT ($C_7H_5N_3O_6$)	F	6.38 e-5	0.162	-1184
	R	7.30 e-5	0.0653	-292
	P	18.3 e-5	-0.213	-746
SDF_1 ($45\%\,C_4H_8N_8O_8; 35\%\,Al; 20\%\,C_4H_6$)	F	-1.54 e-5	0.647	-2358
	R	8.25 e-5	0.0499	-353
	P	18.2 e-5	-0.245	-715
SDF_2 ($17\%\,C_5H_8N_4O_{12}; 17\%\,Al; 66\%\,2CH_2$)	F	19.45 e-5	0.193	-1438
	R	3.39 e-5	0.167	-179
	P	8.17 e-5	-0.0756	-763
SDF_3 ($29\%\,C_4H_8N_8O_8; 15\%\,Al; 56\%\,C_3H_7NO_3$)	F	9.84 e-5	0.143	-1873
	R	8.51 e-5	0.0308	-238
	P	14.3 e-5	-0.132	-485
SDF_4 ($40\%\,Mg; 60\%\,C_3H_7NO_3$)	F	1.17 e-5	0.511	-2751
	R	8.43 e-5	0.0255	-322
	P	12.1 e-5	-0.0772	-555